

Emulating an Atomic Gyroscope with Multiple Accelerometers

Nathan Shettell^{1,*} and Rainer Dumke^{1,2}

¹Centre for Quantum Technologies, National University of Singapore, Singapore 117543, Singapore

²School of Physical and Mathematical Sciences, Nanyang Technological University, 637371, Singapore

*nathans@nus.edu.sg

ABSTRACT

The main advantage of an atomic accelerometer when compared to a classical accelerometer is negligible bias drift, allowing for stable long-term measurements, which opens the potential application in navigation. This negligible drift arises from the fact that the measurements can be traced back to natural constants, and the system is intrinsically stable due to the simple design. In this manuscript, we extend this property of long-term stability to gyroscopic measurements by considering an array of atomic accelerometers, and comparing the performance to atomic gyroscopes, which are technologically more prone to bias drifts. We demonstrate that an array consisting of four three-axis atomic accelerometers can outperform state of the art atomic gyroscopes with respect to long-term stability.

Introduction

Atomic interferometry has undergone rapid technological developments in the past few decades^{1–4}, leading to highly sophisticated technologies that can be used for a variety of precision measurements, including, but not limited to, Earth’s gravity^{5–9}, the fine structure constant^{10,11} and the Aharonov–Casher effect¹². Another promising application of atomic interferometers is navigation and inertial sensing^{13–20}, i.e. as an accelerometer or gyroscope. The main justification for atomic navigation devices (as opposed to a classical device) is that the precision of the measurement can rival the best (classical) inertial sensors^{16,21–23} while maintaining accuracy for a much longer period of time.

Bias drifts are a common hindrance to classical sensors, mainly due to temperature dependencies within the hardware, mechanical wear-and-tear, and aging, which ultimately degrade the accuracy of long-term measurements. In comparison, the measurements taken with atomic accelerometers are based on very well-known and controlled scale factors: the inter-pulse duration, laser wavelength and transition energies, which allows, in principle, for long-term absolute measurements^{6,7,15,24,25}. Unfortunately, not all atomic sensors are created equally, and despite atomic gyroscopes depending on the same aforementioned factors, the mechanical and optical setup is more complex, consequently, the atom trajectory drifts over time, limiting the long-term stability^{26–28}. Atomic gyroscopes, which are suited for navigation (high interrogation rate, broad dynamic range) exhibit bias drifts on the order of $10^{-5} - 10^{-7} \text{ rad}\cdot\text{s}^{-1}/\text{day}$ ^{13,17,27,29–33}; it has been proposed that the ultimate limit is constrained to $\sim 7 \times 10^{-8} \text{ rad}\cdot\text{s}^{-1}/\text{day}$ because of wavefront aberrations and off-resonant Raman transitions^{26,27}. Although progress has been made in terms of features, e.g. compactness, reduced dead-time and multi-axis measurements, improved long-term stability is crucial for commercial viability. Notably, atomic gyroscopes with very long interrogations times ($\sim 0.8 \text{ s}$) and narrow bandwidths have made very impressive strides for long-term stability^{34,35} reporting a bias-drift as low as $2 \times 10^{-9} \text{ rad}\cdot\text{s}^{-1}/\text{day}$ ³⁵. However, because these devices are tailored to a specific measurement, they are not compatible for navigation.

In this work, we explore the prospect of measuring rotational motion with sufficiently many atomic accelerometers^{36–39}, and thus increase the stability of long-term gyroscopic measurements. It is worthwhile to note that using multiple atomic accelerometers does not multiplicatively increase the technological overhead, for example, the same laser system and control electronics can be used for multiple sensor heads. Such a contraption would provide a complete navigational description (linear and rotational motion) using a sole type of technology, facilitating maintenance and troubleshooting. Atomic accelerometers vary drastically in size and performance, but the working principle is the same: an atomic cloud with discrete energy states is stimulated by a sequence of laser pulses, the final state of the atoms will have accumulated a phase proportional to the acceleration parallel to the trajectory of the atoms⁴. A thorough explanation of the underlying physics can be found in Ref.⁵. As we are investigating this idea from a theoretical perspective, the atomic accelerometers are considered to be a blackbox which outputs an estimate of the linear acceleration with statistical constraints (precision, sensitivity, resolution, stability, et cetera).

This work is organized as follows. We begin by outlining the pertinent mathematics to an array of atomic accelerometers (AAA). Next, we compare the performance of an AAA to current atomic gyroscopes^{28,29,32,33}. This is done by considering

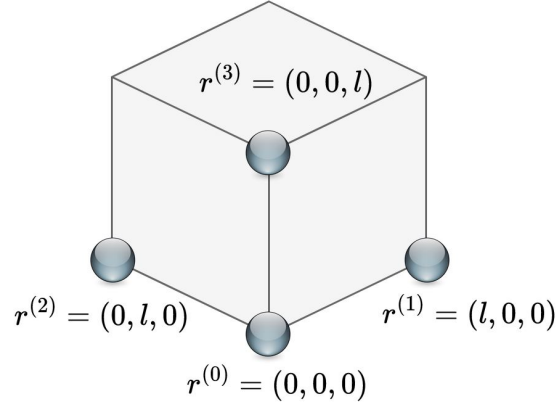


Figure 1. This figure illustrates the AAA we focus on in this study: the location of one central accelerometer is denoted the origin and the other three are each placed along a separate axis at a distance l from the origin. We assume that the atomic accelerometers are simultaneously sensitive to three different axis of acceleration. Although such devices exist, the measurements are sequential and not simultaneous^{13,20,47}, however, assuming the time delay between measurements is small, than this approximation may still hold. Alternatively, one can use a different setup with single-axis atomic accelerometers placed strategically⁴² and obtain simultaneous measurement results.

accelerometers with realistic resolutions^{20,40,41} and subjecting the array to different degrees of rotational motion. We investigate how a bias drift within the atomic accelerometers translates to an effective bias drift with respect to the angular velocity measurement. Additionally, we incorporate expected technical challenges, such as size limitations, positional uncertainties, and misalignment, to determine their effects on the attainable resolution.

Array of accelerometers

Within a rigid body, the difference of linear acceleration (in the rotating reference frame) observed at locations $\mathbf{r}^{(1)}$ and $\mathbf{r}^{(2)}$ is given by

$$\mathbf{a}^{(1)} - \mathbf{a}^{(2)} = W(\mathbf{r}^{(1)} - \mathbf{r}^{(2)}), \quad (1)$$

where

$$W = \dot{\Omega} + \Omega^2, \quad (2)$$

with

$$\Omega = \begin{pmatrix} 0 & \omega_z & -\omega_y \\ -\omega_z & 0 & \omega_x \\ \omega_y & -\omega_x & 0 \end{pmatrix}, \quad (3)$$

and $\boldsymbol{\omega} = (\omega_x, \omega_y, \omega_z)$ is the angular velocity of the rigid body and $\dot{\Omega} = \frac{\partial \Omega}{\partial t}$. It follows that, with sufficiently many accelerometers one can measure the linear acceleration at different locations on the rigid body and reverse engineer said measurements to determine the angular velocity $\boldsymbol{\omega}$ ^{36-39,42,43}. In fact, this idea has been demonstrated using classical sensors for biomechanics^{44,45}.

A minimum of nine single-axis accelerometers are needed to infer the symmetric terms of W (angular velocity) as well as the anti-symmetric terms (angular acceleration). Because of the quadratic nature of Ω^2 , any estimate of $\boldsymbol{\omega}$ has intrinsic sign ambiguity, however this can be eliminated using dependencies between $\boldsymbol{\omega}$ and $\dot{\boldsymbol{\omega}}$ ⁴⁶. In this manuscript we focus on an array of four three-axis atomic accelerometers: where the placement of one of the accelerometers is deemed the origin, and each one of the remaining accelerometers is fixed at a distance l along a separate axis, as depicted in Figure 1. This choice is made for mathematical simplicity, nevertheless, much of the analysis can be straightforwardly adopted to arrays of nine single-axis accelerometers⁴², or of arbitrarily large arrays.

We use the notation $\hat{\square}$ to denote an estimated quantity, e.g. \hat{W} is the estimate of W . There are numerous methods of formulating the estimate $\hat{\boldsymbol{\omega}}$ from \hat{W} ^{48,49}, most of them diverge when one or more components of $\boldsymbol{\omega}$ approaches zero⁵⁰. The methodology we adopt is proposed in Ref.⁴⁸, where one considers the diagonal terms of W in a rotated reference frame,

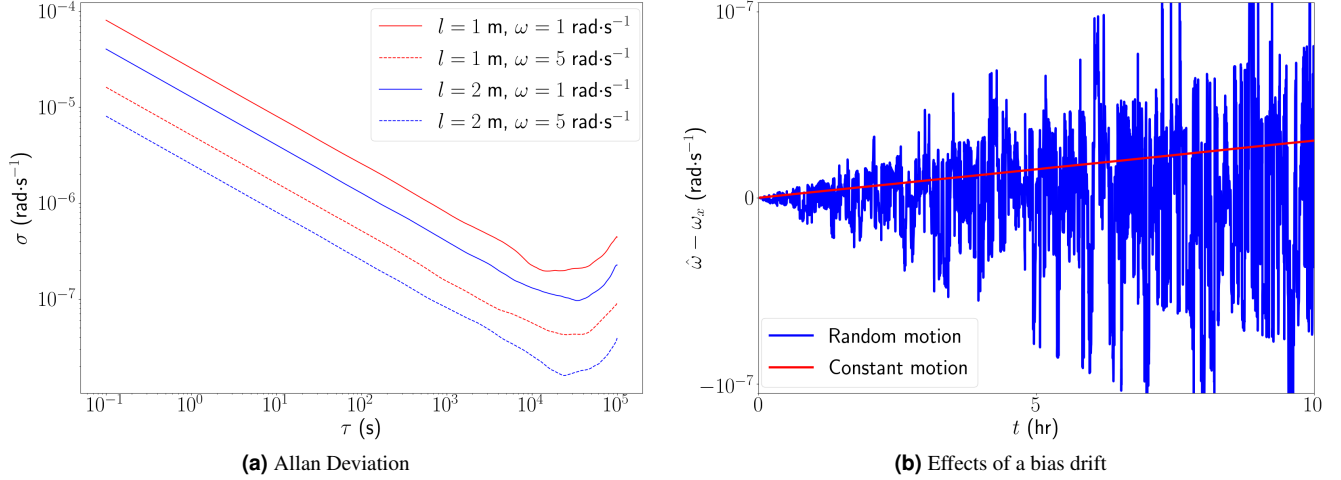


Figure 2. (a) Long-term stability analysis for the angular velocity measurement, in which the accelerometers are subjected to a bias with a drift rate of $6 \times 10^{-7} \text{ ms}^{-2}/\text{day}$. The accelerometers are subjected to a constant rotation of $\boldsymbol{\omega} = \omega(1, 1, 1)/\sqrt{3}$ with $\omega = 1 \text{ rad}\cdot\text{s}^{-1}$ and $\omega = 5 \text{ rad}\cdot\text{s}^{-1}$, and are separated by a distance $l = 1 \text{ m}$ or $l = 2 \text{ m}$. The total Allan deviation $\sigma = (\sigma_x^2 + \sigma_y^2 + \sigma_z^2)^{1/2}$ is plotted, where $\sigma_x, \sigma_y, \sigma_z$ are the Allan deviations corresponding to their respective vector component of $\hat{\boldsymbol{\omega}}$. (b) Error analysis of $\hat{\omega}_x$, for $l = 1 \text{ m}$ and $\|\boldsymbol{\omega}\| = 1 \text{ rad}\cdot\text{s}^{-1}$. The white noise terms, $\boldsymbol{\eta}^{(i)}$, are omitted to highlight the effects of the bias drift. When the array undergoes constant rotation, the drift behaves similarly to a traditional inertial sensor, however, when the array undergoes random motion, the effective drift behaves as white noise which increases in severity with time.

specifically a reference frame where each component of $\boldsymbol{\omega}$ has equal magnitude. This method attains a high degree of precision and diverges solely when $\boldsymbol{\omega}$ tends to exactly zero⁴⁸. An a priori estimate $\tilde{\boldsymbol{\omega}}$ is required to determine the correct reference frame, this can be achieved using a classical sensor, or alternatively, one can use the angular acceleration measurement to construct a self-contained estimation strategy

$$\tilde{\boldsymbol{\omega}}(t_n) = \hat{\boldsymbol{\omega}}(t_{n-1}) + \frac{\Delta t}{2} (\hat{\boldsymbol{\omega}}(t_{n-1}) + \hat{\boldsymbol{\omega}}(t_n)), \quad (4)$$

where t_n is used to denote an estimate of a quantity at the n th measurement and Δt is the time between measurements.

Long-term stability of $\hat{\boldsymbol{\omega}}$

In order to properly compare the long-term stability of the angular velocity measurement made by an AAA, we model the statistical properties of the atomic accelerometers from Ref.²⁰. Namely a single-shot measurement resolution of $7.6 \times 10^{-5} \text{ ms}^{-2}$, and a bias drift of $5.9 \times 10^{-7} \text{ ms}^{-2}/\text{day}$. The data is modeled using

$$\hat{\boldsymbol{a}}^{(i)} = \boldsymbol{a}^{(i)} + \boldsymbol{\eta}^{(i)} + \beta^{(i)} \boldsymbol{u}^{(i)}, \quad (5)$$

where $\boldsymbol{\eta}^{(i)}$ is a random variable to emulate white noise, $\beta^{(i)}$ is the bias of the i th sensor and $\boldsymbol{u}^{(i)}$ is a unit vector signifying the direction in which the accelerometer drifts towards. To simulate the dynamical properties of the drift, the bias at the n th time step, $\beta^{(i)}(t_n)$, is sampled from a normal distribution centered around $\beta^{(i)}(t_{n-1}) + \dot{\beta} \Delta t$, where $\dot{\beta} = 5.9 \times 10^{-7} \text{ ms}^{-2}/\text{day}$ is the drift rate.

In this simulation, the AAA is subjected to constant motion $\boldsymbol{\omega} = \omega(1, 1, 1)/\sqrt{3}$ for time $T = 2 \times 10^6 \text{ s}$, with a sampling time of $\Delta t = 0.1 \text{ s}$. Note that for (most) classical inertial sensors, bias drifts are gauged by performing long-term static measurements; thus, the bias drifts are modeled to be independent of the degree of motion. This is not true for an AAA because of the non-linearity present in the method in which $\hat{\boldsymbol{\omega}}$ is constructed. There is an inverse dependency on the angular velocity, $\|\boldsymbol{\omega}\|$, as well as the separation of atomic accelerometers l . Hence, the simulation is repeated for different values of ω and l .

As a consequence of the subtraction in Eq. (1), the severity of the bias ultimately depends $\boldsymbol{u}^{(i)} - \boldsymbol{u}^{(j)}$. Hence, if two accelerometers drift in the same direction, the quantity $\hat{\boldsymbol{a}}^{(i)} - \hat{\boldsymbol{a}}^{(j)}$ will not induce any drift on the gyroscopic measurements. On the other hand, the effective bias drift will be largest when $\boldsymbol{u}^{(i)} = -\boldsymbol{u}^{(j)}$. For the particular layout we are simulating, see Figure 1, the worst case scenario occurs when the bias of each axial sensor is opposite to the central sensor, which is what we consider in the simulation, Figure 2a.

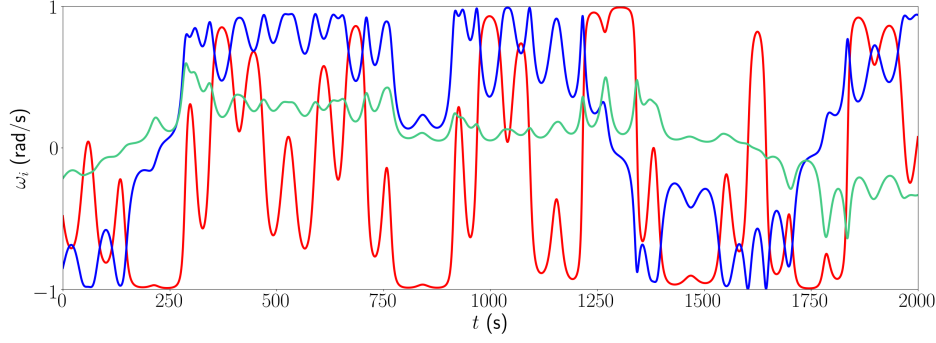


Figure 3. The simulated random values used for ω_x (red), ω_y (blue) and ω_z (green), scaled such that $\|\boldsymbol{\omega}\| = 1$.

Regardless of the values of $\boldsymbol{\omega}$ and l , we find that the bias becomes the limiting factor in accuracy after approximately $T \approx 3 \times 10^4$ s of interrogation. For $\boldsymbol{\omega} = 5 \text{ rad}\cdot\text{s}^{-1}$, the effective bias drift exhibited in the angular velocity measurements is $4.3 \times 10^{-8} \text{ rad}\cdot\text{s}^{-1}/\text{day}$ when $l = 2 \text{ m}$ and $1.2 \times 10^{-7} \text{ rad}\cdot\text{s}^{-1}/\text{day}$ when $l = 1 \text{ m}$. For $\boldsymbol{\omega} = 1 \text{ rad}\cdot\text{s}^{-1}$, the effective bias drift exhibited in the angular velocity measurements is $2.9 \times 10^{-7} \text{ rad}\cdot\text{s}^{-1}/\text{day}$ when $l = 2 \text{ m}$ and $4.3 \times 10^{-7} \text{ rad}\cdot\text{s}^{-1}/\text{day}$ when $l = 1 \text{ m}$. The first three values listed surpass the capabilities of state of the art atomic gyroscopes^{28,29,32,33}, where the best reported value is $3.5 \times 10^{-7} \text{ rad}\cdot\text{s}^{-1}/\text{day}$ ³². Moreover, the $l = 2$ and $\boldsymbol{\omega} = 5 \text{ rad}\cdot\text{s}^{-1}$ result surpasses the hypothesized limit of $\sim 7 \times 10^{-8} \text{ rad}\cdot\text{s}^{-1}/\text{day}$ ^{26,27}. It is worthwhile to note that these values are obtained by simulating the worst case scenario where the bias drifts of the radial sensors occur in the exact opposite direction to the central sensor; on average one expects an improvement by a factor of $\sqrt{2}$.

Evidently, when $\|\boldsymbol{\omega}\|$ is increased, then the effective bias drift is reduced. One technique which could ensure this to be the case, is to subject the AAA to a fixed rotation with angular velocity $\boldsymbol{\omega}_0$ such that $\|\boldsymbol{\omega}_0\| \gg 0$. If the unknown angular velocity is negligible in comparison, i.e. $\|\boldsymbol{\omega}_0 + \boldsymbol{\omega}\| \approx \|\boldsymbol{\omega}_0\|$, then $\|\boldsymbol{\omega}_0\|$ will dictate the bias drift present within the measurements.

Notably, drifting accelerometers has a vastly different effect on $\hat{\boldsymbol{\omega}}$ when the motion is not constant, as portrayed in Figure 2b. When $\boldsymbol{\omega}$ is kept fixed, the effective drift behaves as expected, however, for random motion (see Figure 3) the effective drift behaves as white noise which becomes progressively more severe as time increases.

Resolution analysis

In this section we gauge how different technical challenges inherit to an AAA influence its resolution, namely size limitations, positional uncertainties of the individual sensors, and misalignment of the sensor heads. In all of the simulations, the AAA is subjected to random motion, shown in Figure 3, where $\|\boldsymbol{\omega}\|$ is kept fixed.

Because of the non-linearity of the estimation, it is difficult to determine exact statistical tendencies. Regardless, one can still easily deduce a guideline for the error

$$\|\hat{\boldsymbol{\omega}} - \boldsymbol{\omega}\| \propto \frac{\|\hat{\boldsymbol{a}} - \boldsymbol{a}\|}{Nl\|\boldsymbol{\omega}\|}. \quad (6)$$

Evidently, the capabilities of deducing rotational motion will be bounded by the effectiveness of the accelerometers, hence the proportionality to $\|\hat{\boldsymbol{a}} - \boldsymbol{a}\|$, and similarly improves with the number of accelerometers within the array (N). Moreover, the precision of the apparatus increases when the acceleration on different sensors vary substantially, which is achieved for large values of $\|\boldsymbol{\omega}\|$, or can be artificially achieved by increasing the distance between sensors (l).

Size Limitations

The first aspect we explore is how the size of the AAA affects the attainable resolution. Here, the data is simply simulated using

$$\hat{\boldsymbol{a}}^{(i)} = \boldsymbol{a}^{(i)} + \boldsymbol{\eta}^{(i)}, \quad (7)$$

in which different values of l is considered.

Figure 4a clearly exhibits the hypothesized tendencies for the resolution of the array of atomic accelerometers, Eq. (6), in which the error $\|\hat{\boldsymbol{\omega}} - \boldsymbol{\omega}\|$ is computed for a variety of values for l and $\|\boldsymbol{\omega}\|$. Even for very large arrays with $l = 2.0 \text{ m}$, the attainable single-shot resolution of $\sim 10^{-5} \text{ rad}\cdot\text{s}^{-1}$ is greatly outperformed by state of the art atomic gyroscopes, whose single-shot resolution is on the order of $\sim 10^{-8} - 10^{-9} \text{ rad}\cdot\text{s}^{-1}$ ³⁵. The single-shot resolution of the AAA can be improved upon by introducing additional accelerometers, however, the most practical way of rivaling atomic accelerometers is by hybridizing

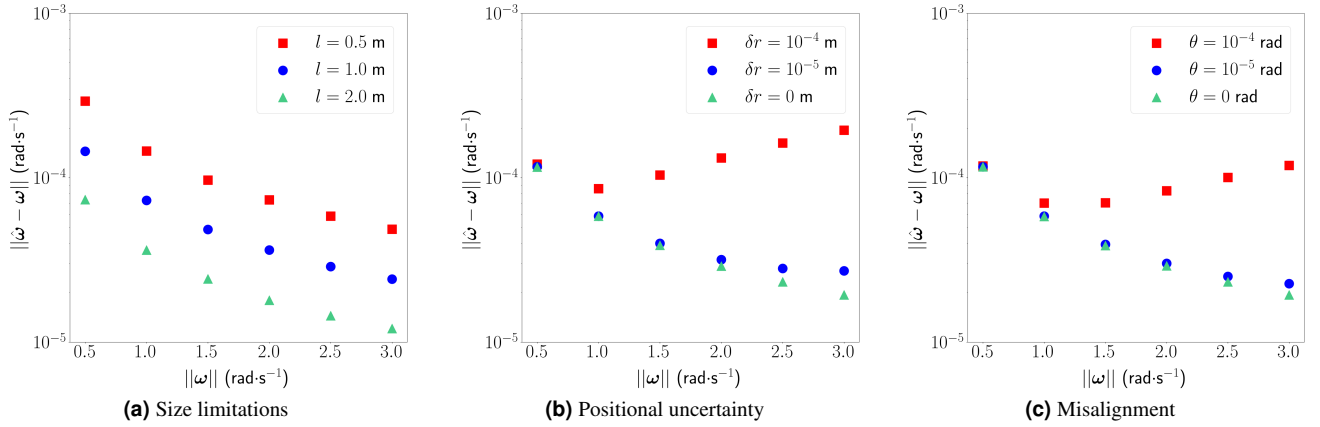


Figure 4. Resolution analysis with respect to different technological challenges inherit to an AAA. In all three plots, the values are obtained by averaging over 25 simulations, this is to consider different values of η , and different directions for the positional uncertainty in (b) and axis of rotation in (c). In each of the 25 simulations, the average error $\|\hat{\omega} - \omega\|$ is computed, where the total interrogation time is $T = 2 \times 10^3$ s and $\Delta t = 0.1$ s. Note that, the error fluctuates minimally in time due to the method in which $\hat{\omega}$ is constructed. (a) Resolution analysis for different sizes of an AAA. (b) Resolution analysis for different degrees of positional uncertainty (with $l = 1.0$ m). (c) Resolution analysis for different degrees of misalignment (with $l = 1.0$ m). The trends in (b) and (c) are similar because a positional uncertainty will induce (with high probability) an angular misalignment; the semblance in numerical values is due to the choice $l = 1.0$ m.

the array of accelerometers with classical sensors^{15,20}; note that this does not defeat the purpose of an AAA, as their most impactful contribution is long-term stability.

Positional Uncertainty

The second aspect we explore is how positional uncertainties in the placement of the individual atomic accelerometers affects the attainable resolution. This positional uncertainty could be caused by fluctuations in the locations of the atomic cloud within the atomic accelerometers. Here, the data is again simulated using Eq. (7), with the addition that the position of the atomic accelerometers, $\mathbf{r}^{(i)}$, are shifted by a distance δr in the direction of a random unit vector $\mathbf{u}^{(i)}$, hence $\mathbf{r}^{(i)} \rightarrow \mathbf{r}^{(i)} + \delta r \mathbf{u}^{(i)}$.

We can deduce from Figure 4b that there is some threshold value for δr , which when surpassed causes the resolution to deviate from the form proposed in Eq. (6). For $l = 1.0$ m, this threshold is between $\delta r = 10^{-4}$ m and $\delta r = 10^{-5}$ m. Moreover, the deviation is exacerbated for larger values of $\|\omega\|$. This threshold can be overcome by incorporating techniques used in gravity gradiometers, where the relative position between atomic clouds are known within $\sim 10^{-9}$ m^{8,9,51}.

Misalignment

The third aspect we explore is how misalignment of the individual atomic accelerometers affects the attainable resolution. The misalignment could be caused by fluctuations in the angle of the retro-reflective mirrors present in the atomic accelerometers, or simply mechanical error when positioning each atomic accelerometer. Here, the data is simulated using

$$\hat{\mathbf{a}}^{(i)} = M_{\theta}^{(i)} (\mathbf{a}^{(i)} + \boldsymbol{\eta}^{(i)}), \quad (8)$$

where $M_{\theta}^{(i)}$ is a matrix which induces a rotation of an angle θ about a random axis.

Similarly to δr , we can deduce from Figure 4c that there is some threshold value for θ , which when surpassed causes the resolution to deviate from the form proposed in Eq. (6). For $l = 1.0$ m, this threshold is between $\theta = 10^{-4}$ rad and $\theta = 10^{-5}$ rad. Fortunately, mechanical alignment can be measured with extremely high-precision, and similarly retro-reflective mirrors are calibrated on the order of $\sim 10^{-6}$ rad⁵ and can be stabilized with extremely precise tilt calibration⁵². Hence, the cumulative misalignment for each atomic accelerometer is not expected to surpass the aforementioned threshold.

Discussion

The long-term stability of atomic accelerometers has greatly improved in the past few decades^{18,19} and currently outclass classical accelerometers. Even though atomic gyroscopes have similarly improved, their long-term stability has not yet surpassed that of classical gyroscopes^{16,18,19}. In this manuscript, we have demonstrated that an array consisting of four three-axis atomic

accelerometers can be an effective substitute for an atomic gyroscope with an order of magnitude improvement over the long-term stability, and even surpass the hypothesized stability limit imposed on atomic gyroscopes^{26,27}. Note that there exists atomic gyroscopes which can surpass the long-term stability of the proposed AAA^{34,35}. However, these require lengthy interrogation times and have a very narrow dynamic range; in this case, a more appropriate comparison would have been to consider analogously designed atomic accelerometers^{7–9,24} in the array.

Unfortunately, an AAA of reasonable size would not be able to match the short-term resolution of atomic gyroscopes. One possible remedy is by using a hybrid system consisting of an atomic accelerometer and a classical gyroscope, utilizing a feedback technique, such as a Kalman filter¹⁵, to achieve long-term stability in addition to high resolution single-shot measurements. Without using feedback from classical sensors, there are four main factors which impact the resolution of angular velocity measurement: the resolution of the accelerometers, the number of accelerometers, the distance between the accelerometers, and the magnitude of the angular velocity. Thus, if one wishes to attain the same resolution with a more compact device, the resolution of the accelerometers must be improved accordingly. In the future, when quantum technologies are more reliable, one could improve the resolution by employing entanglement. By distributing a pair of entangled atoms to the appropriate accelerometers, one could in principle encode the difference of acceleration, $\mathbf{a}^{(i)} - \mathbf{a}^{(j)}$, in the phase of said quantum state. Because of the added statistical correlations, one obtains a $\sqrt{2}$ improvement over the non-entangled strategy⁵³; this is further enhanced when the number of atoms in the entangled state increases. However, the generation of stable entangled quantum states, as well as their distribution, is unfeasible with current quantum technologies.

Our analysis suggests that reducing misalignment and positional uncertainty will be pivotal when designing an AAA, see Figure 4. This is because the error will begin to diverge once either factor surpasses a threshold value. Fortunately, these thresholds can be surpassed with modern technology^{5,51,52,52}.

In this manuscript, we have established the theoretical foundations of using an array of atomic accelerometers as a complete navigational device, i.e. linear and rotational motion. Nonetheless, it is crucial to test the validity with an experimental demonstration. The simplest method would consist of two three-axis atomic accelerometers, which could measure a single vector component of $\boldsymbol{\omega}$, which will suffice as a proof-of-principal demonstration.

References

1. Kasevich, M. & Chu, S. Atomic interferometry using stimulated raman transitions. *Phys. review letters* **67**, 181 (1991).
2. Baudon, J., Mathevet, R. & Robert, J. Atomic interferometry. *J. Phys. B: At. Mol. Opt. Phys.* **32**, R173 (1999).
3. Cronin, A. D., Schmiedmayer, J. & Pritchard, D. E. Optics and interferometry with atoms and molecules. *Rev. Mod. Phys.* **81**, 1051 (2009).
4. Kitching, J., Knappe, S. & Donley, E. A. Atomic sensors—a review. *IEEE Sensors J.* **11**, 1749–1758 (2011).
5. Peters, A., Chung, K. Y. & Chu, S. High-precision gravity measurements using atom interferometry. *Metrologia* **38**, 25 (2001).
6. Bidet, Y. *et al.* Absolute airborne gravimetry with a cold atom sensor. *J. Geod.* **94**, 1–9 (2020).
7. Oon, F. E. & Dumke, R. Compact single-seed, module-based laser system on a transportable high-precision atomic gravimeter. *arXiv preprint arXiv:2208.04174* (2022).
8. Bertoldi, A. *et al.* Atom interferometry gravity-gradiometer for the determination of the newtonian gravitational constant g . *The Eur. Phys. J. D-Atomic, Mol. Opt. Plasma Phys.* **40**, 271–279 (2006).
9. Sorrentino, F. *et al.* Sensitivity limits of a raman atom interferometer as a gravity gradiometer. *Phys. review A* **89**, 023607 (2014).
10. Parker, R. H., Yu, C., Zhong, W., Estey, B. & Müller, H. Measurement of the fine-structure constant as a test of the standard model. *Science* **360**, 191–195 (2018).
11. Morel, L., Yao, Z., Cladé, P. & Guellati-Khélifa, S. Determination of the fine-structure constant with an accuracy of 81 parts per trillion. *Nature* **588**, 61–65 (2020).
12. Sangster, K., Hinds, E., Barnett, S. M. & Riis, E. Measurement of the aharonov-casher phase in an atomic system. *Phys. review letters* **71**, 3641 (1993).
13. Canuel, B. *et al.* Six-axis inertial sensor using cold-atom interferometry. *Phys. review letters* **97**, 010402 (2006).
14. Battelier, B. *et al.* Development of compact cold-atom sensors for inertial navigation. In *Quantum optics*, vol. 9900, 21–37 (SPIE, 2016).
15. Lautier, J. *et al.* Hybridizing matter-wave and classical accelerometers. *Appl. Phys. Lett.* **105**, 144102 (2014).

16. Fang, J. & Qin, J. Advances in atomic gyroscopes: A view from inertial navigation applications. *Sensors* **12**, 6331–6346 (2012).
17. Jiang, L. *et al.* A parametrically modulated dual-axis atomic spin gyroscope. *Appl. Phys. Lett.* **112**, 054103 (2018).
18. Feng, D. Review of quantum navigation. In *IOP Conference Series: Earth and Environmental Science*, vol. 237, 032027 (IOP Publishing, 2019).
19. Geiger, R., Landragin, A., Merlet, S. & Pereira Dos Santos, F. High-accuracy inertial measurements with cold-atom sensors. *AVS Quantum Sci.* **2**, 024702 (2020).
20. Templier, S. *et al.* Tracking the vector acceleration with a hybrid quantum accelerometer triad. *Sci. Adv.* **8**, eadd3854 (2022).
21. Tazartes, D. An historical perspective on inertial navigation systems. In *2014 international symposium on inertial sensors and systems (ISISS)*, 1–5 (IEEE, 2014).
22. El-Sheimy, N. & Youssef, A. Inertial sensors technologies for navigation applications: State of the art and future trends. *Satell. Navig.* **1**, 1–21 (2020).
23. Narducci, F. A., Black, A. T. & Burke, J. H. Advances toward fieldable atom interferometers. *Adv. Physics: X* **7**, 1946426 (2022).
24. Niebauer, T., Sasagawa, G., Faller, J. E., Hilt, R. & Klotting, F. A new generation of absolute gravimeters. *Metrologia* **32**, 159 (1995).
25. Yankelev, D., Avinadav, C., Davidson, N. & Firstenberg, O. Multiport atom interferometry for inertial sensing. *Phys. Rev. A* **100**, 023617 (2019).
26. Fils, J. *et al.* Influence of optical aberrations in an atomic gyroscope. *The Eur. Phys. J. D-Atomic, Mol. Opt. Plasma Phys.* **36**, 257–260 (2005).
27. Gauguet, A. *et al.* Off-resonant raman transition impact in an atom interferometer. *Phys. Rev. A* **78**, 043615 (2008).
28. Gauguet, A., Canuel, B., Lévêque, T., Chaibi, W. & Landragin, A. Characterization and limits of a cold-atom sagnac interferometer. *Phys. Rev. A* **80**, 063604 (2009).
29. Durfee, D., Shaham, Y. & Kasevich, M. Long-term stability of an area-reversible atom-interferometer sagnac gyroscope. *Phys. review letters* **97**, 240801 (2006).
30. Gustavson, T., Landragin, A. & Kasevich, M. Rotation sensing with a dual atom-interferometer sagnac gyroscope. *Class. Quantum Gravity* **17**, 2385 (2000).
31. Stockton, J., Takase, K. & Kasevich, M. Absolute geodetic rotation measurement using atom interferometry. *Phys. review letters* **107**, 133001 (2011).
32. Berg, P. *et al.* Composite-light-pulse technique for high-precision atom interferometry. *Phys. review letters* **114**, 063002 (2015).
33. Yao, Z.-W. *et al.* Calibration of atomic trajectories in a large-area dual-atom-interferometer gyroscope. *Phys. Rev. A* **97**, 013620 (2018).
34. Dutta, I. *et al.* Continuous cold-atom inertial sensor with 1 nrad/sec rotation stability. *Phys. review letters* **116**, 183003 (2016).
35. Savoie, D. *et al.* Interleaved atom interferometry for high-sensitivity inertial measurements. *Sci. advances* **4**, eaau7948 (2018).
36. Padgaonkar, A. J., Krieger, K. & King, A. Measurement of angular acceleration of a rigid body using linear accelerometers. *J. Appl. Mech.* **43** (1975).
37. Madgwick, S. O., Harrison, A. J., Sharkey, P. M., Vaidyanathan, R. & Harwin, W. S. Measuring motion with kinematically redundant accelerometer arrays: Theory, simulation and implementation. *Mechatronics* **23**, 518–529 (2013).
38. Pachter, M., Welker, T. C. & Huffman Jr, R. E. Gyro-free ins theory. *NAVIGATION: J. Inst. Navig.* **60**, 85–96 (2013).
39. Nilsson, J.-O. & Skog, I. Inertial sensor arrays—a literature review. In *2016 European Navigation Conference (ENC)*, 1–10 (IEEE, 2016).
40. Wu, X. *et al.* Multiaxis atom interferometry with a single-diode laser and a pyramidal magneto-optical trap. *Optica* **4**, 1545–1551 (2017).

41. Chen, Y.-J. *et al.* Single-source multiaxis cold-atom interferometer in a centimeter-scale cell. *Phys. Rev. Appl.* **12**, 014019 (2019).
42. Schuler, A. R., Grammatikos, A. & Fegley, K. A. Measuring rotational motion with linear accelerometers. *IEEE transactions on aerospace electronic systems* 465–472 (1967).
43. Carlsson, H., Skog, I., Hendeby, G. & Jaldén, J. Inertial navigation using an inertial sensor array. *arXiv preprint arXiv:2201.11983* (2022).
44. Nusholtz, G. S., Lux, P., Kaiker, P. & Janicki, M. A. Head impact response—skull deformation and angular accelerations. *SAE transactions* 800–833 (1984).
45. Beckwith, J. G., Chu, J. J. & Greenwald, R. M. Validation of a noninvasive system for measuring head acceleration for use during boxing competition. *J. applied biomechanics* **23** (2007).
46. Williams, T. R., Raboud, D. W. & Fyfe, K. R. Minimal spatial accelerometer configurations. *J. Dyn. Syst. Meas. Control.* **135**, 021016 (2013).
47. Barrett, B., Cheiney, P., Battelier, B., Napolitano, F. & Bouyer, P. Multidimensional atom optics and interferometry. *Phys. Rev. Lett.* **122**, 043604 (2019).
48. Cardou, P. & Angeles, J. Angular velocity estimation from the angular acceleration matrix. *J. Appl. Mech.* **75** (2008).
49. Cardou, P., Fournier, G. & Gagnon, P. A nonlinear program for angular-velocity estimation from centripetal-acceleration measurements. *IEEE/ASME Transactions on Mechatronics* **16**, 932–944 (2010).
50. Parsa, K., Lasky, T. A. & Ravani, B. Design and mechatronic implementation of an accelerometer-based, kinematically redundant inertial measurement unit. In *Proceedings, 2005 IEEE/ASME International Conference on Advanced Intelligent Mechatronics.*, 644–651 (IEEE, 2005).
51. D’Amico, G. *et al.* Canceling the gravity gradient phase shift in atom interferometry. *Phys. review letters* **119**, 253201 (2017).
52. Oon, F. E. & Dumke, R. Compact active vibration isolation and tilt stabilization for a portable high-precision atomic gravimeter. *arXiv preprint arXiv:2206.06028* (2022).
53. Giovannetti, V., Lloyd, S. & Maccone, L. Quantum metrology. *Phys. review letters* **96**, 010401 (2006).

Acknowledgements

This research is supported by the DSO National Laboratories. The authors would also like to thank Fong En Oon, Kai Sheng Lee, Elizaveta Maksimova and Christoph Hufnagel for fruitful discussions.

Author contributions statement

N. S. conducted the statistical analysis. All authors reviewed the manuscript.

Additional information

The authors declare no competing interests.